

IRON-LINE EMISSION AS A PROBE OF BARDEEN-PETTERSON ACCRETION DISKS

P. CHRIS FRAGILE

Physics Department, University of California, Santa Barbara, CA 93106

AND

WARNER A. MILLER, ERIC VANDERNOOT

Physics Department, Florida Atlantic University, Boca Raton, FL 33431

Draft version March 17, 2018

ABSTRACT

In this work we show that Bardeen-Petterson accretion disks can exhibit unique, detectable features in relativistically broadened emission line profiles. Some of the unique characteristics include inverted line profiles with sharper red horns and softer blue horns and even profiles with more than 2 horns from a single rest-frame line. We demonstrate these points by constructing a series of synthetic line profiles using simple two-component disk models. We find that the resultant profiles are very sensitive to the two key parameters one would like to constrain, namely the Bardeen-Petterson transition radius r_{BP} and the relative tilt β between the two disk components over a range of likely values [$10 \leq r_{BP}/(GM/c^2) \leq 40$; $15^\circ \leq \beta \leq 45^\circ$]. We use our findings to show that some of the “extra” line features observed in the spectrum of the Seyfert-I galaxy MCG-6-30-15 may be attributable to a Bardeen-Petterson disk structure. Similarly, we apply our findings to two likely Bardeen-Petterson candidate Galactic black holes - GRO J1655-40 and XTE J1550-564. We provide synthetic line profiles of these systems using observationally constrained sets of parameters. Although we do not formally fit the data for any of these systems, we confirm that our synthetic spectra are consistent with current observations.

Subject headings: accretion, accretion disks — black hole physics — galaxies: active — galaxies: Seyfert — line: profiles — X-rays: stars

1. INTRODUCTION

Relativistically broadened emission lines have been observed in the X-ray spectra of over a dozen active galactic nuclei (AGN) (Mushotzky et al. 1995; Tanaka et al. 1995; Nandra et al. 1997). More recently similar features have also been discovered in Galactic black holes (GBHs) and black hole candidates (Miller et al. 2002a,b,c). These lines, from fluorescent $K\alpha$ emission of iron, provide a unique diagnostic of the inner regions of accretion flows around black holes. Such fluorescent lines are produced when hard X-rays illuminate regions of optically thick disk material (George & Fabian 1991; Matt et al. 1991). Since the line energies are well known (6.4 keV for cold iron with ionization states below Fe XVII, 6.7 keV for Fe XXV, and 6.9 keV for Fe XXVI) and the intrinsic widths are very small, the observed, broadened line profiles can provide direct information on the Doppler shifts and gravitational redshifts affecting the line-emitting material (Fabian et al. 1989; Laor 1991). If one assumes the emitting gas to be in the form of a thin Keplerian disk, then these line profiles also provide information on the emissivity of the disk, the radial distribution of the emitting gas, and the observed inclination angle i of the disk ($i = 0^\circ$ is face on) (Laor 1991; Pariev & Bromley 1998; Pariev et al. 2001). The profiles of these lines are also sensitive to features of more realistic disk models such as turbulent broadening and radial inflow (Pariev & Bromley 1998; Armitage & Reynolds 2003).

The dependence of these line profiles on the radius of emission and inclination of the disk suggest that they may be useful as a diagnostic of warped or twisted accretion disks (Hartnoll & Blackman 2000). One such warping

mechanism which is active at small radii around rapidly rotating black holes is caused by relativistic Lense-Thirring precession. Here the frame dragging of the rotating black hole causes orbits that are inclined (or tilted) with respect to the spin axis of the black hole to precess. For test particles, the precession frequency is $\Omega_{LT} = 2GMa/(c^2r^3)$. For a tilted disk, the Lense-Thirring precession causes a radially dependent torque which, by itself, would cause the disk to twist up. However, in a disk this twisting must compete with whatever angular momentum transport mechanism (i.e. “viscosity”) is driving the accretion. In such a case, the quasi-steady-state solution is characterized by a two-component disk with the inner disk aligned with the symmetry plane of the black hole and the outer disk essentially retaining its original orientation (as set by the angular momentum of the gas reservoir). This is the so-called Bardeen-Petterson effect (Bardeen & Petterson 1975). It is characterized in terms of a tilt angle β between the inner and outer disk components and a transition radius r_{BP} where the two components connect.

If iron lines are emitted by the disk, then depending on where the lines are emitted relative to the Bardeen-Petterson transition radius, the resulting line profile may reveal unique *detectable* spectral features characterizing one or both disk components. First, if r_{BP} lies within the line emitting region, part of the line flux will be emitted at one inclination relative to the observer while the remainder will be emitted at a different inclination. Since the blue wing ($g_{max} = \nu_{max}/\nu_e$) of a broadened line profile is sensitive to the inclination of the emitting region, a tilted, two-component disk could produce multiple blue horns from a single (rest-frame) line. The red tail ($g_{min} = \nu_{min}/\nu_e$)

would also be sensitive to a Bardeen-Petterson disk since it is responsive to the inner radius of the emitting region, which would obviously be different for an inner and outer disk component. The observer would see an integrated line profile that is in effect a superposition of the line profiles from the two disk components (minus any reduction in flux due to shadowing). Thus, as we will show, Bardeen-Petterson disks can exhibit unique spectral features not seen in flat single-disk models, such as inverted line profiles with sharper red horns and a softer blue horns or even profiles with more than 2 horns from a single (rest-frame) line.

Perhaps the most important possible outcome of this research would be to directly constrain the scale of the Bardeen-Petterson transition radius through observations. There is currently great uncertainty as to where the transition radius is likely to lie, with estimates varying from $r_{BP} \lesssim 20r_g$ (Nelson & Papaloizou 2000) to $r_{BP} \geq 100r_g$ (Bardeen & Petterson 1975), where $r_g \equiv GM/c^2$ is the gravitational radius of the black hole. The expectation is that it will occur approximately where the rate of twisting by differential Lense-Thirring precession is balanced by the rate at which twists are diffused or propagated away by viscosity. The large uncertainty in r_{BP} then is largely a product of our ignorance of the details of angular momentum transport in accretion disks, particularly in tilted disks where the vertical shear component of viscosity may be crucial. Constraining r_{BP} through observations would go a long way toward improving our understanding of black hole accretion disks.

Even if r_{BP} lies outside the line-emitting region, the presence of a Bardeen-Petterson disk could still be inferred in some cases. For instance, the tilted outer disk may shadow parts of the inner line-emitting region. The observable signatures of such shadowing was explored in Hartnoll & Blackman (2000), although for somewhat different scales than are considered here. Furthermore, the Bardeen-Petterson effect provides a natural explanation for why fits of some iron lines require inclinations that appear inconsistent with other observations of the same system. This is seen more often in GBHs where the inclination of the binary is often well constrained. For instance, the best-fit models for the iron line in V 4641 Sgr give an inclination of $i = 43^\circ \pm 15^\circ$ (Miller et al. 2002b), whereas the optically determined inclination (of the far outer disk) is $60^\circ \lesssim i \leq 71^\circ$ (Orosz et al. 2001). Although these inclination measurements are marginally consistent with one another, a true discrepancy of this type could easily be reconciled if one assumes that the iron line comes from the inner component of a two-component Bardeen-Petterson disk.

We consider a range of values for the tilt β between the disks, with magnitudes in the range $0^\circ \leq |\beta| \leq 45^\circ$. For GBHs, $\beta \lesssim 30^\circ$ is consistent with expectations based upon the formation avenues of compact binaries (cf. Fragile et al. 2001). It is also consistent with the currently available observational constraints on such systems. For instance, as noted above, the best-fit models for the iron line in V 4641 Sgr give an inclination of $i = 43^\circ \pm 15^\circ$ (Miller et al. 2002b), whereas the optically determined inclination is $60^\circ \lesssim i \leq 71^\circ$ (Orosz et al. 2001), yielding a possible tilt between the outer disk and the inner iron-line-

emitting region of $\beta > 2^\circ$ (as we discuss below, the upper limit is uncertain because the orientation of the observer relative to the line-of-nodes is unknown). Interestingly, the radio jet observed from this source forms an angle with the line-of-sight of $\theta < 6^\circ$ (Orosz et al. 2001). If the axis of this jet is coincident with the spin axis of the black hole or the angular momentum of the inner accretion flow, as is commonly assumed, then the tilt could be quite large, $\beta > 54^\circ$. A similar, although less extreme, discrepancy is observed between the jet and disk inclinations in GRO J1655-40 (Fragile et al. 2001; Orosz et al. 2001), where the jet lies almost in the plane of the sky ($\theta = 85^\circ \pm 2^\circ$, Hjellming & Rupen 1995) and the disk has an inclination $i = 70.2^\circ \pm 1.9^\circ$ (Greene et al. 2001), suggesting a possible tilt of $\beta \gtrsim 15^\circ$. Another example is found in XTE J1550-564, for which the apparent superluminal motion of its radio jets (Hannikainen et al. 2001), constrains θ to be $< 53^\circ$ while the observed inclination of the outer disk is $i = 72.2^\circ \pm 5.2^\circ$, again suggesting a possible tilt of $\beta \gtrsim 14^\circ$.

The case for Bardeen-Petterson disks around supermassive black holes is less clear. Nevertheless, many supermassive black holes are thought to be spinning rapidly (Elvis et al. 2002; Yu & Tremaine 2002) and two plausible scenarios for supplying the necessary tilted accretion flow come to mind: 1) episodic accretion from tidally disrupted transiting objects, such as is thought to fuel the accretion of Sgr A*, the supermassive black hole at the center of the Milky Way; or 2) accretion following galactic merger events where the supermassive black hole has not had sufficient time to align with the accreting matter. Neither case would appear to have a preferred orientation and thus presents the possibility of a full range of tilts.

The main goal of this paper is to highlight some of the unique features expected in relativistically broadened iron-lines emitted by Bardeen-Petterson disks. Although this is a highly idealized study, we show in §2 that the profiles are quite sensitive to the Bardeen-Petterson disk parameters. Observations of such lines could therefore be used to set meaningful constraints on the physics of Bardeen-Petterson disks. In §3, we proceed to discuss our results in terms of a few selected GBHs and AGN. We also illustrate that this technique for studying Bardeen-Petterson disks through relativistically broadened line profiles will be most successful when combined with other observations that can help constrain the system parameters.

2. IMAGING AND LINE PROFILES OF BARDEEN-PETTERSON DISKS

2.1. Disk Model

We model the Bardeen-Petterson effect very simplistically as two separate infinitesimally thin disks: an inner disk extending from r_{in} to r_{BP} and an outer disk extending from r_{BP} to r_{out} . For most of our models we assume the black hole to be maximally rotating so that $a/M = Jc/GM^2 = 1$. In this case, the formal cut-off for the disk at the last stable orbit coincides with the horizon of the black hole, i.e. $r_{ms} = r_{BH} = r_g$. However, we effectively truncate the disk at $r_{in} = 1.05r_{BH}$ by terminating photon trajectories that penetrate this radius. This is done for numerical convenience as the integration times of the photon trajectories become infinitely long as they approach the horizon. The choice of $a/M = 1$ was made

somewhat arbitrarily, and although this value cannot be reached by an astrophysical black hole, we demonstrate below that reducing a/M does not cause any more dramatic change to our results than those attributed to other uncertainties in our models.

The outermost disk radius is set to $r_{out} = 100r_g$. The transition radius is varied over the range $10 \leq r_{BP}/r_g \leq 40$, consistent with the numerical results of Nelson & Papaloizou (2000). In such a simple two-component Bardeen-Petterson disk model, we expect separate red and blue horns to be produced by each disk component. This is where the power of this technique lies. Since the blue horns will be sensitive to the relative tilt of the two disks and the red horns will be sensitive to the location of the transition radius, the full line profile gives information about the two parameters one would most like to constrain.

All of the models in this work assume a twist-free disk (i.e. the line-of-nodes of the two disks is a straight line). Based upon numerical simulations (Nelson & Papaloizou 2000) this seems consistent with expectations for a Bardeen-Petterson disk. We generalize our results by allowing the observer to be placed anywhere on a sphere of large radius ($500r_g$). The observer's location is described by two angles $\{\theta_0, \phi_0\}$, in the usual Boyer-Lindquist spherical coordinates centered on the black hole. Since the observer's location is often unconstrained, we consider a range of choices for θ_0 and ϕ_0 . However, as we show in §3.1, if the inclination of the inner or outer disk relative to the observer can be constrained, then the observer's location is no longer arbitrary.

2.2. Ray Tracing

To obtain an image of the accretion disk as seen by a distant observer, we integrate the geodesic equations of motion using a variant of the numerical ray tracing code described in Bromley et al. (1997). We follow the trajectories of photons from a pixelated grid of points at some large distance ($r = 500r_g$) back to the accretion disk. The uniform grid may be associated with the field imaged by a CCD detector for instance. The observed frequency at each pixel is given by

$$g \equiv \frac{\nu_o}{\nu_e} = \frac{-1}{-u \cdot p}, \quad (1)$$

where subscripts o and e are observer and emitter, respectively, u is the 4-velocity of the emitter, and p is the emitted photon's 4-momentum. Generally, the emitter 4-velocity is specified by the disk model. In this work we simply use the Keplerian 4-velocity in the plane of the disk, ignoring effects such as radial transport and turbulent motion which have been explored in a general context elsewhere (Pariev & Bromley 1998). The photon 4-momentum is tracked while numerically tracing the photon geodesic back in time from the observer's grid to the surface of the disk (inner or outer). We discard photons that are intercepted by the black hole or otherwise miss the disk. Thus we properly account for the role of the black hole in absorbing photons emitted near the horizon. Here we assume that the transition region connecting the two disks is optically thin (i.e. photons passing between the two disk components near the transition radius don't "hit" anything). The validity of this assumption depends on the width of the transition zone and upon how much

material on average is present within the transit region, neither of which is known at this time.

In this work we also ignore the illumination of the disk by line photons emitted in other parts of the disk and the possible reflection of those photons to the observer. Because of uncertainties in the emissivity function and the fact that the flux in the line is a small fraction of the X-ray continuum in this energy range, this is probably reasonable. Nevertheless, in future work we plan to explore the effect of line reprocessing in Bardeen-Petterson disks.

2.3. Line Profiles

From the pixelated disk image, we generate a synthetic line profile by making a histogram of the number of pixels in different frequency bins. Each frequency bin is an accumulation of the contributions of individual pixels and thus represents an integral over the disk. The actual flux comes from weighting each bin by the emissivity $\epsilon(r)$ and g^4 ; three factors of g coming from the relativistic invariant I_ν/ν^3 , where I_ν is the intensity, and the remaining factor arising because the line profile is an integrated flux. This weighting takes care of the effects of Doppler motions and gravitational redshifts. The emissivity $\epsilon(r)$ is the *local* emissivity in the frame of the disk. Since some fraction of the photons emitted close to the black hole will be captured by it, $\epsilon(r)$ does not correspond directly to the energy received by the distant observer.

Throughout this paper we cast our results in terms of a 6.4 keV rest-frame line energy. However, nothing in our methodology is tied to this value. In this sense our results would be equally valid for any other spectral line that might be emitted from the region of the disk studied here. However, as will become clear, our results would be considerably confused if two or more lines were emitted with rest-frame energies separated by $\Delta E/E \lesssim 0.2$. This could be particularly troublesome in accretion disks with a mixture of H-like, He-like, and cold iron.

Throughout this work we assume an emissivity of the form $\epsilon(r) \propto r^{-q}$ and generally use $q = 2.5$. This is steeper than the r^{-2} expected for a centrally illuminating source, yet shallower than the r^{-3} expected from local energy dissipation within a disk. Obviously a shallower radial dependence would increase the flux contribution of the outer disk, whereas a steeper radial dependence would decrease it. Regardless, provided a detectable amount of flux is emitted by both disk components, our results will be qualitatively insensitive to the choice of q since the locations (in frequency or energy) of the red and blue horns are insensitive to the specific flux distribution (Cunningham 1975). However, the strength of each feature, and hence its detectability, *will* depend upon the value of q . We explore this dependence further below.

Other details of our results may also depend on the form of the emissivity function we have chosen. For instance, in the case of a central compact source (or in so-called "lamppost" models), the change in the angle of incidence of the illuminating radiation beyond r_{BP} would cause a change in the slope of $\epsilon(r)$. Accounting for such effects would require tracing the photon trajectories from their originating source, which is not done in the current work.

Before considering specific black-hole systems, we first explore how our synthetic line profiles depend on the various parameters of interest. We start by testing the de-

pendence of such profiles on the tilt angle β between the two disks. We consider four models with values of β in the range $0 \leq \beta \leq 45^\circ$. For all of these models, the transition radius is set to $r_{BP} = 15r_g$, the inclination between the observer and the outer disk is fixed at $i_{out} = 45^\circ$, and the observer is located at $\phi_0 = 90^\circ$ (perpendicular to the line-of-nodes). Figure 1 shows both the image of the disk and the line profile for the $\beta = 30^\circ$ case. For illustration, we have plotted the line profiles of each disk component separately as well as the composite line profile. This gives a good feel for how the remainder of the line profiles are generated. Figure 2 shows the composite line profiles for the four models with varying β . Clearly the $\beta \neq 0$ cases are easily distinguishable. The most prominent signature of the Bardeen-Petterson profiles is the presence of an "extra" horn, contributed by the inner disk component. Since the observer remains fixed relative to the outer disk in all these models, the blue edge g_{max} , which is controlled here by the outer disk, remains fixed. However, the extra blue wing from the inner disk is sensitive to the tilt β . In these models, a larger β translates into a smaller inclination for the inner disk which, in turn, results in the corresponding blue horn becoming redder. In fact, for the most tilted case considered, the blue horn of the inner disk (located at $g \approx 0.84$) is found at a lower energy than the red horn of the outer disk (located at $g \approx 0.92$). The key point, though, is that the separation of the various horns is a sensitive indicator of the tilt between the two disk components. In other words, measuring this separation provides a direct constraint on β , although, as we show below, this conclusion does depend on the observer's location relative to the line-of-nodes.

Next, we explore the dependence of a set of synthetic Bardeen-Petterson line profiles on the scale of the transition radius r_{BP} . For these models, β remains fixed at 30° and the observer is located at $\{\theta_0 = 15^\circ, \phi_0 = 90^\circ\}$, giving inclinations of 15° and 45° between the observer and the inner and outer disk components, respectively. Figure 3 shows the line profiles for five values of r_{BP} in the range $10 \leq r_{BP}/r_g \leq 40$. For these models, it is not the blue horn that shows the greatest variability, but rather the red horn. Thus, while the blue horn is sensitive to the tilt β between the disks, the red horn is sensitive to the transition radius r_{BP} . This is because the red horn closely tracks the inner radius of a given disk component. Since increasing r_{BP} is equivalent in our models to increasing the inner radius of the outer disk component, varying the transition radius causes a noticeable shift in the red horn of the outer disk from $g \approx 0.76$ for $r_{BP} = 10r_g$ to $g \approx 0.92$ for $r_{BP} = 40r_g$. Note that for the set of parameters considered here, the inner disk does not exhibit a red horn; however, even if it did, it would not be very sensitive to a change in the transition radius since the minimum radius of the inner disk component would not change. Varying the transition radius also changes the amount of flux coming from the inner and outer disk components, so that the relative amplitudes of the various horns provides another diagnostic of Bardeen-Petterson disks. A final point to emphasize from Figure 3 is that the Bardeen-Petterson effect causes *detectable* changes in the iron line profile even when $r_{BP} \geq 40r_g$. This is an important result, although as we show below, it is somewhat dependent on form of

the emissivity function.

Next we vary the black hole spin parameter a . Although the Bardeen-Petterson transition radius is expected to be a function of a , in this work we treat them as independent parameters so that r_{BP} remains fixed at $15r_g$ for the current set of models. The remaining parameters are also held at their canonical values ($\beta = 30^\circ$, $i_{out} = 45^\circ$, $\phi_0 = 90^\circ$, and $q = 2.5$). Line profiles for four values of a/M between 0.5 and 1 are shown in Figure 4. The biggest effect of changing a is that the inner radius of the disk r_{in} (assumed equal to r_{ms}) moves to larger radii for smaller a ($r_{ms} = 1, 1.24, 2.32$, and 4.23 for $a/M = 1, 0.998, 0.9$, and 0.5 , respectively). Since photons are not emitted from as deep in the potential well for larger r_{in} , the flux in the red tail is greatly diminished. Overall the flux contribution of the inner disk component is also reduced due to its decreased surface area.

So far we have only considered observers with a line-of-sight perpendicular to the line-of-nodes ($\phi_0 = 90^\circ$). However, the line profile for a given Bardeen-Petterson disk will depend on the specific location of the observer, so we now consider a set of line profiles made from the same Bardeen-Petterson disk configuration, but seen from different viewing angles. To do this, we maintain a constant inclination between the observer and the outer disk while shifting the value of ϕ_0 . Effectively, the observer is circling the angular momentum axis of the outer disk. For these models, the tilt, transition radius, and inclination of the outer disk relative to the observer remain fixed at $\beta = 30^\circ$, $r_{BP} = 15r_g$, and $i_{out} = 45^\circ$. The observer is shifted through 180° from the positive y -axis ($\phi_0 = 90^\circ$) to the negative y -axis ($\phi_0 = -90^\circ$). Figure 5 shows the resulting line profiles. The most noticeable change is the dramatic shift in the blue horn attributed to the inner disk, which ranges from $g \approx 0.81$ for $\phi_0 = 90^\circ$ to $g \approx 1.35$ for $\phi_0 = -90^\circ$. The contribution from the outer disk, on the other hand, remains roughly constant since the observer maintains a constant orientation with respect to this component and the transition radius remains fixed; therefore, the red and blue horns attributed to the outer disk are always located near $g \approx 0.92$ and $g \approx 1.05$, respectively. Nevertheless, there are still small changes in the outer disk contribution due mostly to shadowing by the inner disk. Thus far the results have shown that an iron line profile can be a sensitive probe for determining the relative tilt between two components of a Bardeen-Petterson disk and the radius at which the two components meet. However, these results have all assumed an emissivity of the form $\epsilon(r) \propto r^{-q}$ with $q = 2.5$. Although this is a reasonable choice based upon theoretical expectations and is consistent with some fitted line profiles, it is by no means the only plausible choice. Other values of q are certainly possible, as are other functional forms for ϵ (e.g. the "lamp-post" model is a popular alternative). We finish this section by considering a few other choices of q . Figure 6 illustrates how the line profiles vary for choices of q from 0 to 3. In all models, $\beta = 30^\circ$, $r_{BP} = 15r_g$, $i_{out} = 45^\circ$, and $\phi_0 = 90^\circ$. For $q \leq 2$, the results are sensitive to our choice of r_{out} , which remains fixed at $100r_g$ in all cases. The profiles are normalized by the flux in the blue horn. It is clear from the figure that for $q \lesssim 1$ the large outer disk component swamps the emission from the inner disk.

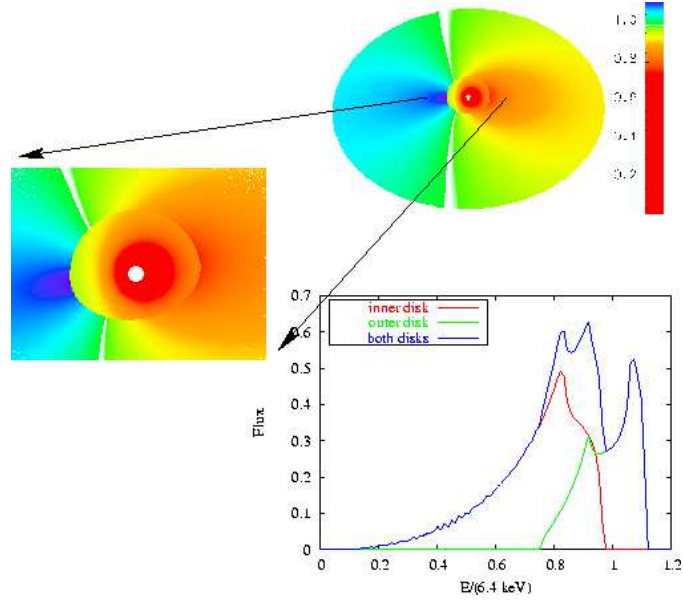


FIG. 1.— Example disk image of a two-component Bardeen-Petterson disk with $\beta = 30^\circ$ and $r_{BP} = 15r_g$. The observer is located at $\phi_0 = 90^\circ$ (line-of sight perpendicular to the line-of-nodes) and is inclined 45° with respect to the outer disk and 15° with respect to the inner disk.

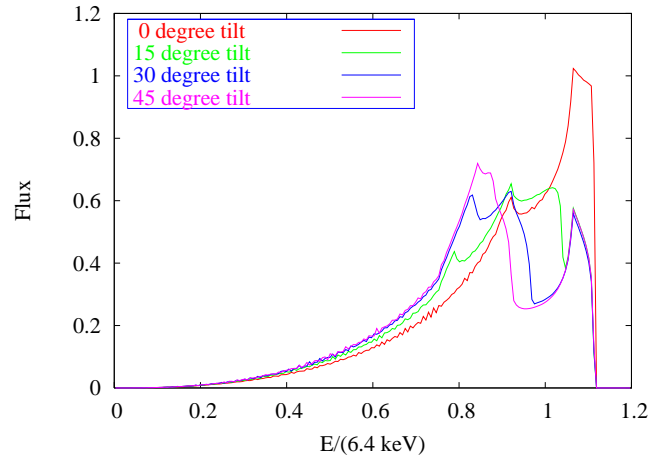


FIG. 2.— Synthetic line profiles for a sample of two-component Bardeen-Petterson disks with $r_{BP} = 15r_g$ and various values for the tilt β in the range $0 \leq \beta \leq 45^\circ$. The observer is located at $\phi_0 = 90^\circ$ and maintains a constant inclination of $i_{out} = 45^\circ$ with respect to the outer disk.

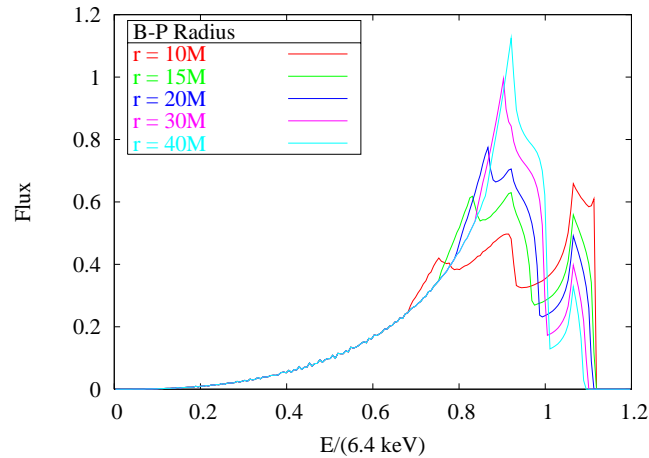


FIG. 3.— Synthetic line profiles with the tilt fixed at $\beta = 30^\circ$ and the transition radius varied over the range $10 \leq r_{BP} \leq 40$. The observer is located at $\phi_0 = 90^\circ$ and is inclined 45° with respect to the outer disk and 15° with respect to the inner disk.

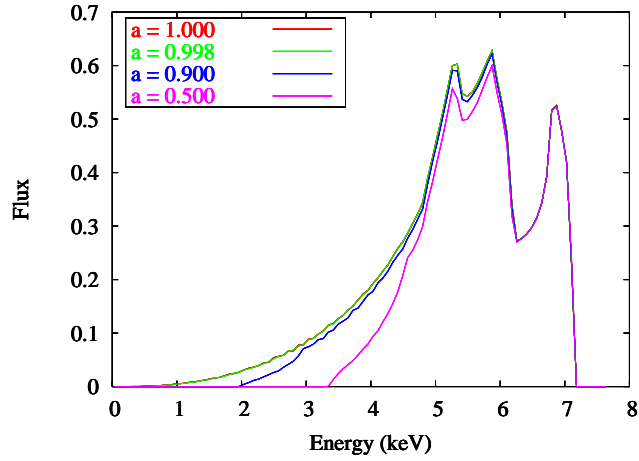


FIG. 4.— Synthetic line profiles with the tilt, transition radius, longitude of the observer, and inclination of the observer relative to the outer disk fixed at $\beta = 30^\circ$, $r_{BP} = 15r_g$, $\phi_0 = 90^\circ$, and $i_{out} = 45^\circ$, respectively. The emissivity assumes a form $\epsilon(r) \propto r^{-q}$, with $q = 2.5$. The spin of the black hole is varied over the range $0.5 \leq a/M \leq 1$.

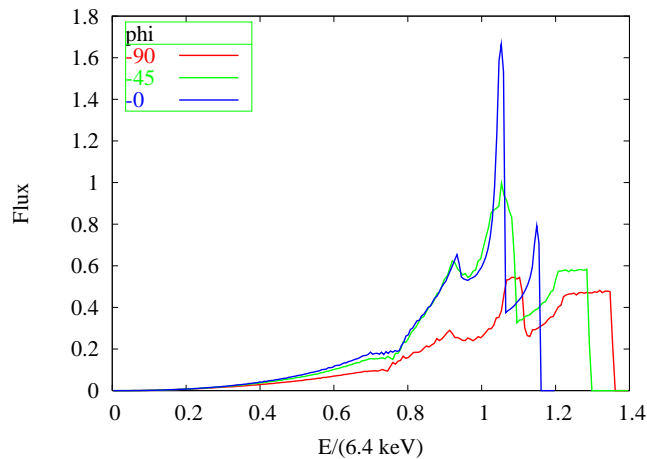
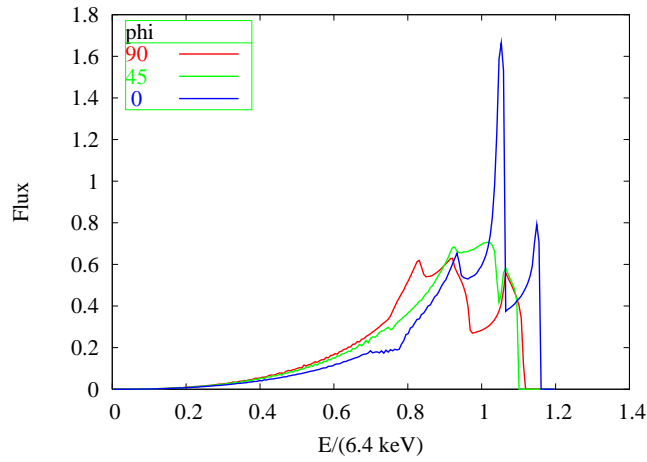


FIG. 5.— Synthetic line profiles with the tilt, transition radius, and inclination of the observer relative to the outer disk fixed at $\beta = 30^\circ$, $r_{BP} = 15r_g$, and $i_{out} = 45^\circ$, respectively. The longitude of the observer is varied over the range (a) $0 \leq \phi_0 \leq 90$ and (b) $-90 \leq \phi_0 \leq 0$.

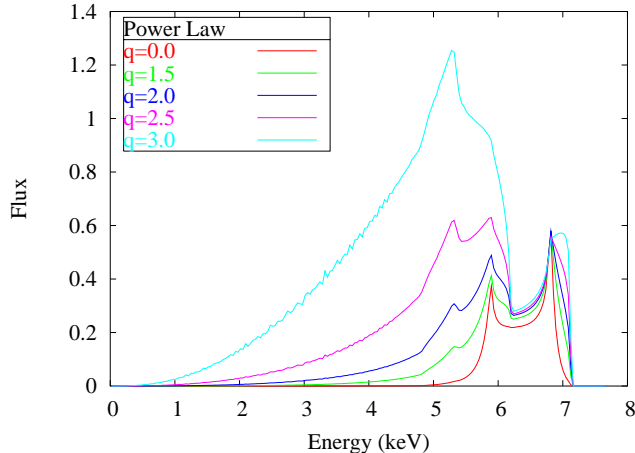


FIG. 6.— Synthetic line profiles with the tilt, transition radius, longitude of the observer, and inclination of the observer relative to the outer disk fixed at $\beta = 30^\circ$, $r_{BP} = 15r_g$, $\phi_0 = 90^\circ$, and $i_{out} = 45^\circ$, respectively. The emissivity assumes a form $\epsilon(r) \propto r^{-q}$, with the numerical value of q varied from 0 to 3. All of these profiles are normalized using the peak flux in the blue horn at $E = 6.7$. The normalization factors are 2.73×10^4 , 50, 6.73, 1, and 0.157 for $q = 0, 1.5, 2.0, 2.5$, and 3.0, respectively.

Only for steeper power-laws does the inner disk contribution become apparent. If we were to continue this exercise to consider even steeper power-laws, the inner disk component would eventually swamp the outer disk contribution. It is in the intermediate region, when both disk components are detectable, that this technique is most useful as a probe of Bardeen-Petterson disks. The exact range of q for which this will be true will depend on many parameters including r_{min} , r_{BP} , r_{max} , and the inclination of the observer relative to the two disk components. Nevertheless, we have shown that this technique should work for a reasonable range of choices of all parameters.

3. IMPLICATIONS FOR GALACTIC BLACK HOLES AND SEYFERT GALAXIES

In the previous section, we showed that iron-line profiles could, in principle, be used as a diagnostic of Bardeen-Petterson disks. Useful science could be extracted from such profiles in the form of constraints on the relative tilt of Bardeen-Petterson disks and on the location of the transition radius. However, the practical effect of including the Bardeen-Petterson effect in modeling of iron-line profiles is to add three new free parameters that must be fit: two new parameters come from the tilt β and transition radius r_{BP} , themselves, and the third new parameter comes from replacing a single inclination angle i with the two angles $\{\theta_0, \phi_0\}$ necessary to describe the observer's location relative to the two disk components. Given the many uncertainties already inherent in fitting relativistically broadened lines, this is not an entirely attractive prospect. Nevertheless, we discuss some examples where there may be compelling reasons to make the effort.

3.1. Galactic Black Holes

Often the inclination i of an X-ray binary orbit can be determined through careful observation and fitting of the photometric light curve, the radial velocity curve, and other observables (e.g. rotational velocity of the secondary), when the system is in X-ray quiescence. In cases where the primary black hole is a microquasar, the spin axis of the black hole can be inferred from the orientation

of the relativistic jet, which makes an angle θ_{jet} with respect to the line-of-sight of the observer. If both i and θ_{jet} are reasonably constrained, then the position of the observer (θ_0, ϕ_0) in our models is confined to the family of points satisfying

$$\begin{aligned} \theta_0 &= \theta_{jet} \\ \sin \phi_0 &= \frac{\cos i - \cos \beta \cos \theta_{jet}}{\sin \beta \sin \theta_{jet}} \end{aligned} \quad (2)$$

where we have utilized the law of cosines on a sphere. In this way, we can remove one of the extra degrees of freedom required to fit a Bardeen-Petterson disk, leaving only the dependencies on β and r_{BP} . At this time, this approach probably gives the best hope for constraining the Bardeen-Petterson transition radius. (Spectral modeling of the continuum may also provide important constraints.) Following this procedure, we discuss two GBHs that are likely candidates for Bardeen-Petterson disks and provide sample synthetic line profiles of each. For now these synthetic line profiles are illustrative in nature since we do not fit actual observations. However, we do discuss the qualitative similarities between our synthetic lines and actual line profiles in the literature (Balucińska-Church 2001; Miller et al. 2004).

3.1.1. GRO J1655-40

GRO J1655-40 is one of the best studied and most tightly constrained GBHs, with a binary period of 2.62191 ± 0.00020 days, a primary (black-hole) mass of $6.3 \pm 0.5 M_\odot$, and a binary inclination of $i = 70.2 \pm 1.9^\circ$ (Greene et al. 2001). It has also been previously identified as a likely candidate for a Bardeen-Petterson disk (Fragile et al. 2001). This characterization comes from noting the discrepancy between the binary inclination and the orientation of the highly collimated bipolar relativistic jet seen in this source during a 1994 outburst ($\theta_{jet} = 85 \pm 2^\circ$; Hjellming & Rupen 1995). If we assume that the orientation of the jet is fixed by the angular momentum axis of the black hole, then the tilt between the binary orbital plane and the black hole symmetry plane is $\beta \geq 10.9^\circ$. Due to the remaining degree of freedom to select the precise location of the observer (i.e. choosing ϕ_0 in our models), we

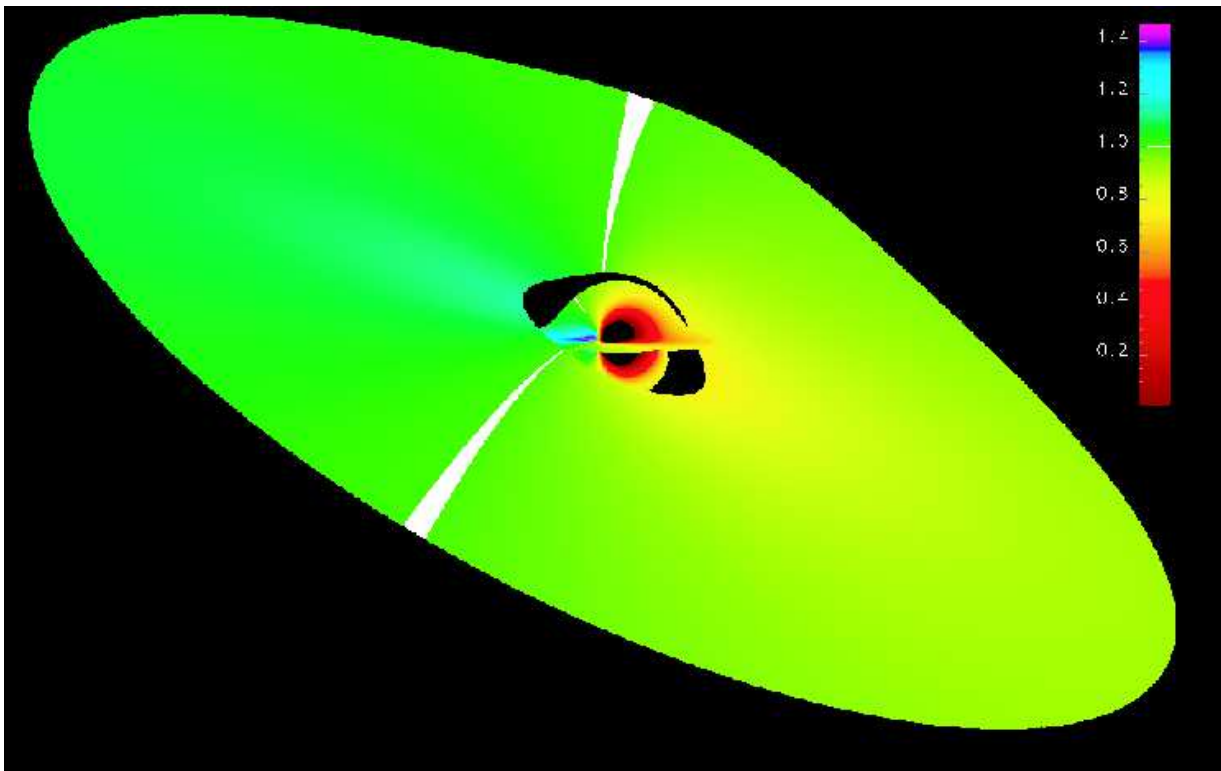


FIG. 7.— Disk image of GRO J1655-40 for an observer at $\{\theta_0, \phi_0\} = \{85^\circ, 32^\circ\}$ ($\beta = 30^\circ$). Using observational constraints we fix the inclinations of the inner and outer disk components at $i_{in} = 85^\circ$ and $i_{out} = 70.2^\circ$, respectively. The transition radius is set at $r_{BP} = 15r_g$.

can not place a tight upper limit on the tilt. The formal upper limit is $\beta \leq (180 - 10.9)^\circ = 169.1^\circ$. Nevertheless, we argue on physical grounds that $\beta \leq 30^\circ$ is probably a reasonable upper limit. For instance, values of $\beta > 90^\circ$ would imply that the inner disk is orbiting in the opposite sense of the outer disk. Although such large tilts may be possible in some systems (e.g. systems that have undergone binary capture or binary replacement), such counter-rotating disks seem a highly unlikely scenario. In fact, it is hard to imagine that a Bardeen-Petterson disk structure could be supported if β were much larger than about 45° , as this would require a dramatic reorientation of the angular momentum of the gas in the transition region. Adopting a limit of $\beta \leq 30^\circ$ and using equation 2 to fix the observer's location $\{\theta_0, \phi_0\}$, we consider two possible tilt angles for GRO J1655-40: $\beta = 15^\circ$ and 30° . The corresponding observer locations are $\{\theta_0, \phi_0\} = \{85^\circ, 81^\circ\}$ and $\{85^\circ, 32^\circ\}$. In both cases, the inclinations of the inner and outer disks are $i_{in} = 85^\circ$ and $i_{out} = 70.2^\circ$, respectively, consistent with the observations. Thus the inner disk is viewed more edge on than the outer disk, although both are viewed from fairly low latitudes, as shown in the disk image in Figure 7. Notice that the inner disk is viewed from such a low latitude that photons from the bottom of the disk are bent enough to propagate through the gap at the transition radius and make it to the observer. Although this is an interesting illustration of light-bending effects, it also highlights the limitations of our assumptions of an infinitesimally thin disk and an optically thin transition radius. In a real system, these photons would likely be blocked from view by the flaring of the disk or optically thick gas in the transition region. Nevertheless, we include

these photons in the synthetic line profiles shown in Figure 8. The four lines in the figure correspond to the two observer locations and two values for the transition radius: $r_{BP} = \{15, 30\}r_g$. All of the models assume a maximally rotating black hole, an outer radius of $r_{max} = 100M$, an observer at $r = 500M$, and a disk emissivity of the form $\epsilon \propto r^{-2.5}$. The noise in the profiles is a result of the poor resolution of the inner disk, which again is seen nearly edge-on.

The peak in the synthetic line profile at $E \approx 7$ keV is attributable to the blue horn of the outer accretion disk component overlaid on the much broader line from the inner disk. The energy of this peak is very close to the peak line energy seen in the *ASCA* observations of this source (Miller et al. 2004). Assuming a rest-frame line energy of 6.4 keV, this observed line energy requires a disk inclination of $i \gtrsim 45^\circ$, consistent with all other indications that this system is seen at high inclination. Rest-frame line energies of 6.7 or 6.9 keV (from highly ionized iron) could be fit with smaller inclinations, but would require the emitting region to be far from the hole.

The extremely high inclination of our model inner disk leads to a very large value for the blue maximum ($g_{max} = 1.5$ or $E_{max} = 9.4$ keV for a 6.4 keV line), below which there is a shallow blue plateau. Although such high-energy line emission is not apparent in the observed spectrum of GRO J1655-40 (Miller et al. 2004), this does not necessarily rule out a highly inclined inner disk component. Such a component could be present, yet have its emission obscured through self-absorption by the finite-thickness of the disk itself (unlike the infinitesimally thin disks considered here). Or it could be that the high-energy line emission is hidden by absorption features. This is a potential problem for all relativistically broadened lines, not just those from Bardeen-Petterson disks. Absorption is particularly problematic at energies above about 7 keV.

3.1.2. XTE J1550-564

XTE J1550-564 has many similarities to GRO J1655-40, although its parameters are generally not as well constrained. Despite the larger uncertainties, it is still clear that the system hosts a black-hole primary ($8.36M_\odot \leq M_1 \leq 10.76M_\odot$). The binary period (1.552 ± 0.010 days) and inclination ($67.0^\circ \leq i \leq 77.4^\circ$) are also reasonably well known. Similar to GRO J1655-40, XTE J1550-564 is a microquasar. During a 1998 outburst, large scale relativistic jets were observed in both X-ray and radio wavelengths (Hannikainen et al. 2001; Corbel et al. 2002). The radio components displayed apparent separation velocities of $> 2c$ (Hannikainen et al. 2001). Although the exact orientation of the jets was not confirmed, the apparent superluminal motion itself constrains the angle of the jet relative to the line-of-sight to be $\theta_{jet} < 53^\circ$. Similar to GRO J1655-40 and V 4641 Sgr, this jet orientation is in disagreement with the inclination of the binary orbit; in this case, the implied tilt is $\beta \geq 14^\circ$. Although the limit on this tilt is very similar to the limit for GRO J1655-40 and the binary inclinations are quite similar, there is a key difference between the two systems: for GRO J1655-40, the implied inner disk is viewed more edge-on than the outer disk, whereas for XTE J1550-564, the orientation is reversed and the outer disk is viewed more edge-on. Since the superluminal motion of the jet only gives us an upper limit on θ , we are unable to use equation 2 to further constrain the observer location for XTE J1550-564. Nevertheless, for illustration, in Figure 9 we assume a jet angle $\theta_{jet} = 45^\circ$ and a tilt $\beta = 30^\circ$. The corresponding observer locations is $\{\theta_0, \phi_0\} = \{45^\circ, -60^\circ\}$. The inclinations of the inner and outer disks are $i_{in} = 45^\circ$ and $i_{out} = 72.2^\circ$, respectively. Again we assume a maximally rotating black hole, an outer radius of $r_{max} = 100M$, an observer at $r = 500M$, and a disk emissivity of the form $\epsilon \propto r^{-2.5}$.

We consider two values of $r_{BP} = \{15, 30\}r_g$. Since the outer disk component for XTE J1550-564 is nearly identical to what we used for GRO J1655-40, it is not surprising that its contribution to the line profiles is quite similar (compare Figures 10 and 8). The differences between the two figures are mainly attributable to the inner disk component and to differences in the shadowing of the various models. The synthetic spectrum of XTE J1550-564 in Figure 10 has a peak at $E \approx 7$ keV. Some of the photons in this peak come from the outer edge of the inner disk component ($i_{in} = 45^\circ$), while the rest come from the inner edge of the outer disk ($i_{out} = 72.2^\circ$). This value is roughly consistent with the peak of the observed line in XTE J1550-564 at $E \approx 6.8$ keV (Miller et al. 2004). For a rest frame energy of 6.4 keV, this requires a disk inclination $i \gtrsim 45^\circ$. For $r_{BP} = 15r_g$, the synthetic spectrum also shows some excess emission in the range $E = 7 - 8$ keV. This comes from the inner edge of the outer disk component and is not seen for $r_{BP} \gtrsim 30r_g$ since the Keplerian velocity of the orbiting gas is not high enough in such a case. Interestingly, excess emission above the continuum fit also appears over the same energy range in the observations of XTE J1550-564 (Miller et al. 2004). Line flux in this energy range requires a disk inclination of $i \gtrsim 60^\circ$, consistent with the binary inclination and the inclination of the outer disk component in our models. Although we have not formally fit the data for XTE J1550-564, it is clear that the observed profile is consistent with a Bardeen-Petterson disk configuration.

3.2. Seyfert Galaxies

Although GBHs may provide the best constrained systems for studying iron-line profiles, at this time their data do not have as high of a signal-to-noise value as the observations of Seyfert 1 galaxies. The high quality of Seyfert 1 data makes it appropriate to at least consider this class of object as part of this study. Furthermore, there is a potential puzzle that a Bardeen-Petterson disk might help rectify: According to the unified model of active galactic nuclei, type 1 Seyfert galaxies are believed to be viewed at low inclination angles ($i \lesssim 30^\circ$) in order that they not be obscured by the dust torus presumed to surround the accretion disks at large radii. However, such low inclinations would prohibit the blue wing of an iron line from extending much above its rest-frame energy ($g_{max} \lesssim 1$). Therefore, the presence of detectable emission above 6.4 keV is a potential problem. It has usually been interpreted as evidence that the emission is coming from highly ionized states of iron (Fe XXIV-XXVI). However, we consider a Bardeen-Petterson profile such as the ones shown in this work to be a potentially more conservative, alternative explanation. In the context of the unified model, the outer disk of a Seyfert 1 galaxy would be required to have a low inclination, but the Bardeen-Petterson model would allow the inner disk to take on a broader range of inclinations. In particular, a higher inclination for the inner disk would allow the blue wing to extend above 6.4 keV without resorting to higher ionization states.

3.2.1. MCG-6-30-15

One of the best studied iron-line sources is the nearby type 1 Seyfert galaxy MCG-6-30-15. It was the first

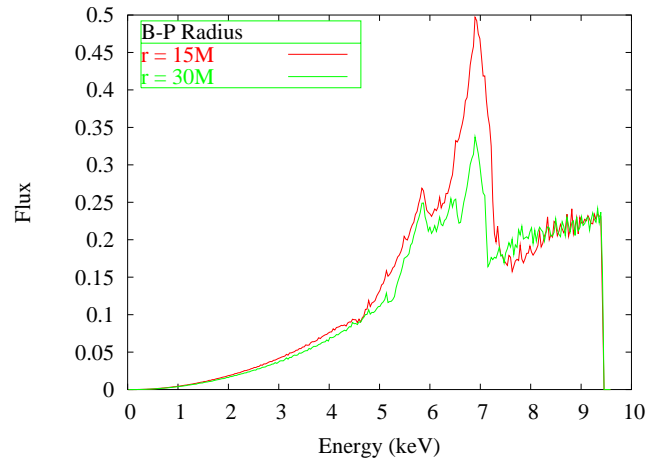
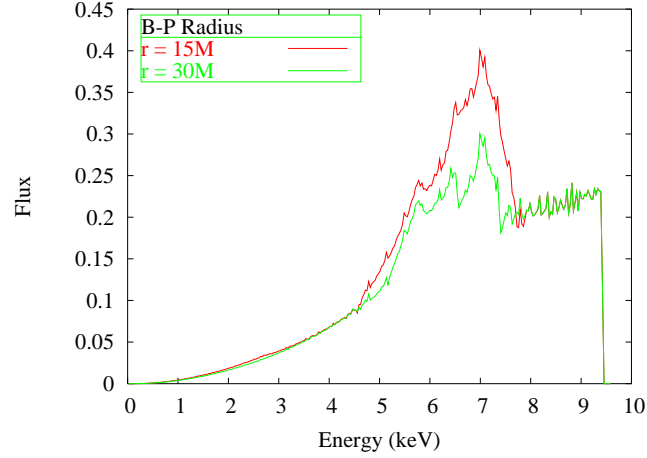


FIG. 8.— (a) Synthetic line profiles for GRO J1655-40 for an observer at $\{\theta_0, \phi_0\} = \{85^\circ, 81^\circ\}$ ($\beta = 15^\circ$) and (b) $\{\theta_0, \phi_0\} = \{85^\circ, 32^\circ\}$ ($\beta = 30^\circ$). In all cases, we assume the black hole is maximally rotating, $r_{max} = 100M$, and $\epsilon \propto r^{-2.5}$. In each case, we present profiles for two values of the transition radius ($r_{BP} = \{15, 30\}r_g$).

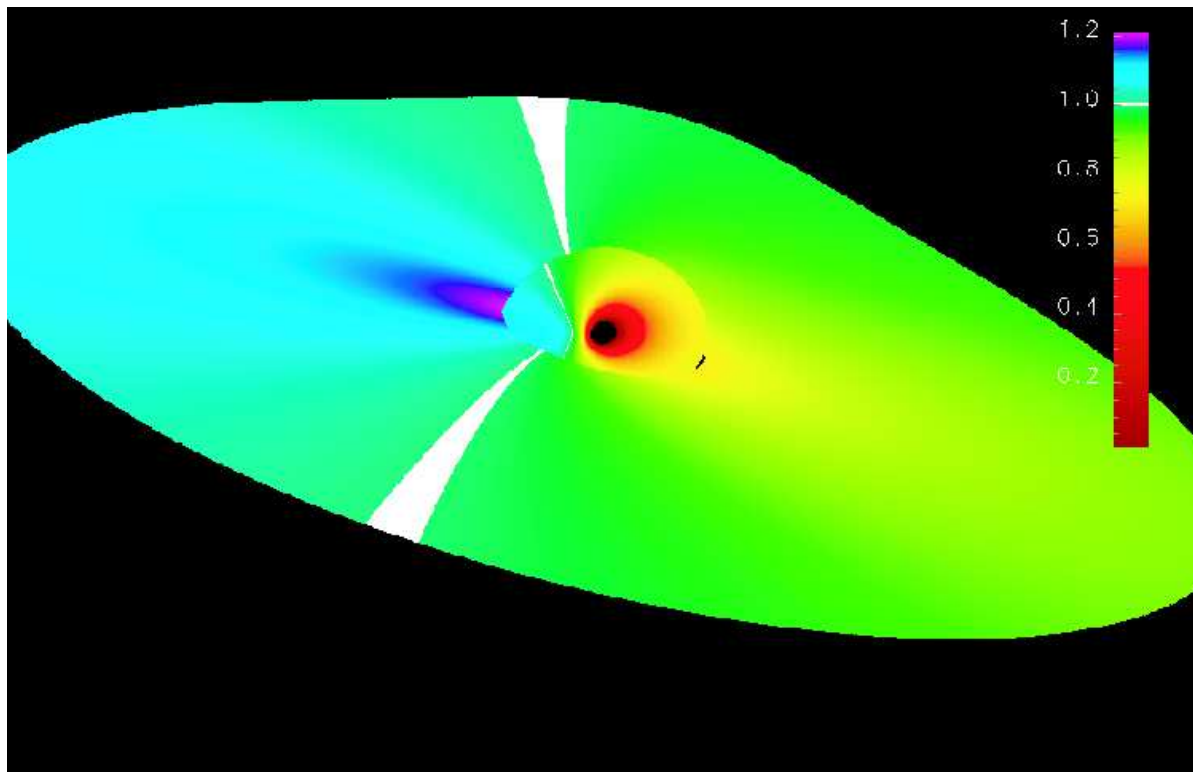


FIG. 9.— Disk image of XTE J1550-564. We use observational constraints to fix the inclinations of the outer disk component at $i_{out} = 72.2^\circ$. We assume the inner disk is inclined $i_{in} = 45^\circ$, consistent with the observational constraint $i_{in} < 53^\circ$. The transition radius is fixed at $r_{BP} = 15r_g$ and the observer is located at $\{\theta_0, \phi_0\} = \{45^\circ, -60^\circ\}$.

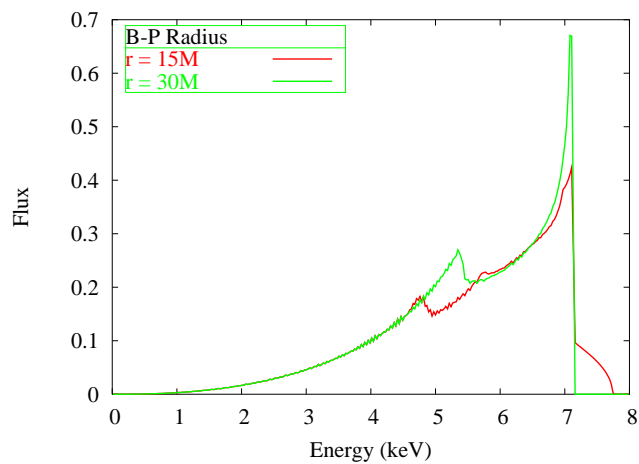


FIG. 10.— Synthetic line profiles for XTE J1550-564. For these, we assume the black hole is maximally rotating, $r_{max} = 100M$, $\epsilon \propto r^{-2.5}$, and $\beta = 30^\circ$. We present profiles for two values of the transition radius ($r_{BP} = \{15, 30\}r_g$).

source to show a relativistically broadened iron-line feature (Tanaka et al. 1995) and remains one of the most cited examples. In fact, the data for this source are of such high quality, they actually reveal a complex set of features that can not be adequately fit as a single line (Fabian et al. 2002; Ballantyne et al. 2003). The key features include a strong, broad peak near 6.4 keV, a very extended red tail down to $E \lesssim 3$ keV, and an “extra” horn or peak near 6.9 keV. As mentioned above, a 6.9 keV emission feature is a potential problem for Seyfert galaxies in the context of the unified model since disks seen at low inclinations (like Seyfert-1s) can not produce strongly blue-shifted lines. Thus this feature is often attributed to highly ionized states of iron (Fe XXIV-XXVI). Alternatively we show that these complex features can be qualitatively explained using a “single” 6.4 keV iron line from a Bardeen-Petterson disk. The key principle is that we can satisfy the unified model of AGN provided we model the outer disk component with a small inclination while we are free to choose a broader range of inclinations for the inner disk. We suggest therefore that, in the case of MCG–6-30-15, it is the outer component that produces the core line near 6.4 keV while an inner disk component produces both the extended red wing and the 6.9 keV feature. In order to do so from a 6.4 keV rest-frame line, the inner disk must be inclined at least 45° with respect to the observer (Pariev et al. 2001). If we assume that the outer disk is inclined 30° , this gives a tilt $\beta \geq 15^\circ$ depending on the angle between the line-of-sight and line-of-nodes ($\beta = 15^\circ$ if $\phi_0 = 90^\circ$; $\beta > 15^\circ$ if $\phi \neq 90^\circ$).

In Figure 11 we show a synthetic line profile that qualitatively matches the data for MCG–6-30-15 (Fabian et al. 2002). This profile assumes the observer’s line-of-sight is perpendicular to the line-of-nodes ($\phi_0 = 90^\circ$) so that the tilt is $\beta = 15^\circ$. Unlike most of our previous models, in which the black hole was maximally rotating, here we assume a spin $a/M = 0.5$, giving an inner disk radius of $r_{min} = 4.2M$. The transition radius is taken to be $r_{BP} = 20M$. As in previous models, we assume an emissivity of the form $\epsilon \propto r^{-2.5}$. We note, however, that this emissivity may not be steep enough to reproduce the observed red wing flux. Nevertheless, it is worth point out that our relatively simple physical model is successful in matching many of the unusual features of the MCG–6-30-15 line profile. As described earlier, a nice property of our model is that it provides a natural explanation for why the flux in the line core of MCG–6-30-15 does not match the flux in the red wing: these two flux contributions come from different disk components with different inclinations relative to the observer (in this case, the outer disk is seen more face on).

4. CONCLUSIONS

We set out in this work to demonstrate that relativistically broadened iron lines can reveal important details about Bardeen-Petterson disks in GBHs and AGN. In support of this goal, we showed that such spectral lines are sensitive to the two parameters of greatest interest in Bardeen-Petterson disks: the tilt between the two disk components and the transition radius where they meet. At this time, this approach probably gives the best hope for determining these parameters, although spectral modeling

of the continuum can also provide some constraints.

We applied our results to a small set of potentially interesting systems. One class of such systems is microquasars. These objects are often better constrained in terms of the relevant parameters than other potential targets such as AGN. Any fits to iron-line profiles in microquasars must be consistent with observations of the binary orbital parameters, the orientation of the relativistic jet, and spectral fitting of the thermal (accretion disk) component. This kind of consistency check will be particularly helpful in ruling out competing effects. Unfortunately, current observations of iron lines from microquasars do not have sufficiently high signal-to-noise to resolve the extra features that are characteristic of Bardeen-Petterson disks. Nevertheless, current or future missions should be able to achieve the required sensitivity. In anticipation of this, we have provided predicted spectra of two likely Bardeen-Petterson microquasar candidates: GRO J1655-40 and XTE J1550-564.

Although AGN are generally not as well constrained as microquasars, they nevertheless represent another important class of objects in the context of this work. Furthermore, they have historically yielded higher quality line profiles. In this work we focused on one example: MCG–6-30-15. Here we showed that a Bardeen-Petterson disk profile could qualitatively explain the complicated line profile observed in that system, *without resorting to extra lines from other ionization states of iron*. Although other models have been proposed that produce similar features, we feel the Bardeen-Petterson explanation is an intriguing possibility. The discovery of a Bardeen-Petterson disk in an AGN would reveal a wealth of information about the environment of the accretion flow and the history of the system.

The most restrictive limitation of this technique is that, to be fully exploited, both components of the Bardeen-Petterson disk must produce detectable levels of line flux. Provided this condition is met, we have shown that the line profiles exhibit unique signatures, such as inverted (red-horn-dominant) lines or lines with more than two horns, that are not easily mimicked by other effects. Nevertheless, there are competing effects one must be aware of. Probably the most important are line blending, for instance from low and high ionization states of iron, and disk warping due to mechanisms other than Lense-Thirring precession. Line blending will be particularly confusing if two or more lines are emitted with rest-frame energies separated by $\Delta E/E \lesssim 0.2$. In such cases, one will have to rely on other observational and physical constraints of the system to disentangle the possibilities.

In closing, we would like to suggest that it might be fruitful in the future to conduct a systematic search for Bardeen-Petterson features among all observations of relativistically broadened iron lines. Such a search could yield important statistical bounds on questions such as: How many systems have tilted accretion disks? What is the average tilt in such systems? What is the average transition radius? Answering these questions will give important clues toward understanding accretion-disk physics and the evolutionary history of accreting black holes.

P.C.F. gratefully acknowledges useful discussion and

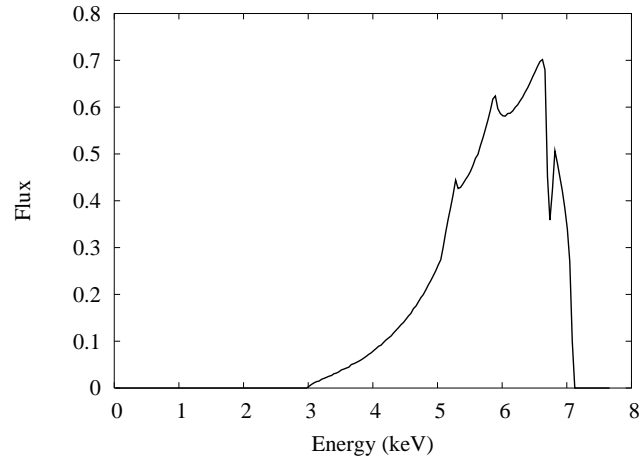


FIG. 11.— Synthetic line profile providing a qualitative fit to MCG–6–30–15. For this model, the disk parameters are $r_{min} = 4.2M$, $r_{BP} = 20M$, $\beta = 15^\circ$, $r_{max} = 100M$, and $\epsilon \propto r^{-2.5}$. The observer is located at $\phi_0 = 90^\circ$ and has inclinations of $i_{out} = 30^\circ$ and $i_{in} = 45^\circ$ with respect to the outer and inner disk components, respectively.

feedback on this work from S. Davis and O. Blaes. We thank the anonymous referee for suggesting important improvements to the manuscript. Funding support for P.C.F.

was provided by NSF grant AST 0307657. W.A.M. wishes to acknowledge support from FAU's Office of Graduate Studies and from an LDRD/ER grant from LANL.

REFERENCES

- Armitage, P. J., & Reynolds, C. S. 2003, *MNRAS*, 341, 1041
 Ballantyne, D. R., Vaughan, S., & Fabian, A. C. 2003, *MNRAS*, 342, 239
 Balucińska-Church, M. 2001, *Advances in Space Research*, 28, 349
 Bardeen, J. M., & Petterson, J. A. 1975, *ApJ*, 195, L65
 Bromley, B. C., Chen, K., & Miller, W. A. 1997, *ApJ*, 475, 57
 Corbel, S., Fender, R. P., Tzioumis, A. K., Tomsick, J. A., Orosz, J. A., Miller, J. M., Wijnands, R., & Kaaret, P. 2002, *Science*, 298, 196
 Cunningham, C. T. 1975, *ApJ*, 202, 788
 Elvis, M., Risaliti, G., & Zamorani, G. 2002, *ApJ*, 565, L75
 Fabian, A. C., Rees, M. J., Stella, L., & White, N. E. 1989, *MNRAS*, 238, 729
 Fabian, A. C., et al. 2002, *MNRAS*, 335, L1
 Fragile, P. C., Mathews, G. J., & Wilson, J. R. 2001, *ApJ*, 553, 955
 George, I. M., & Fabian, A. C. 1991, *MNRAS*, 249, 352
 Greene, J., Bailyn, C. D., & Orosz, J. A. 2001, *ApJ*, 554, 1290
 Hannikainen, D., Campbell-Wilson, D., Hunstead, R., McIntyre, V., Lovell, J., Reynolds, J., Tzioumis, T., & Wu, K. 2001, *Astrophysics and Space Science Supplement*, 276, 45
 Hartnoll, S. A., & Blackman, E. G. 2000, *MNRAS*, 317, 880
 Hjellming, R. M., & Rupen, M. P. 1995, *Nature*, 375, 464
 Laor, A. 1991, *ApJ*, 376, 90
 Matt, G., Perola, G. C., & Piro, L. 1991, *A&A*, 247, 25
 Miller, J. M., Fabian, A. C., in't Zand, J. J. M., Reynolds, C. S., Wijnands, R., Nowak, M. A., & Lewin, W. H. G. 2002a, *ApJ*, 577, L15
 Miller, J. M., Fabian, A. C., Nowak, M. A., & Lewin, W. H. G., preprint (astro-ph/0402101)
 Miller, J. M., et al. 2002b, *ApJ*, 578, 348
 Miller, J. M., et al. 2002c, *ApJ*, 570, L69
 Mushotzky, R. F., Fabian, A. C., Iwasawa, K., Kunieda, H., Matsuoka, M., Nandra, K., & Tanaka, Y. 1995, *MNRAS*, 272, L9
 Nandra, K., George, I. M., Mushotzky, R. F., Turner, T. J., & Yaqoob, T. 1997, *ApJ*, 477, 602
 Nelson, R. P., & Papaloizou, J. C. B. 2000, *MNRAS*, 315, 570
 Orosz, J. A., et al. 2001, *ApJ*, 555, 489
 Pariev, V. I., & Bromley, B. C. 1998, *ApJ*, 508, 590
 Pariev, V. I., Bromley, B. C., & Miller, W. A. 2001, *ApJ*, 547, 649
 Tanaka, Y., et al. 1995, *Nature*, 375, 659
 Yu, Q., & Tremaine, S. 2002, *MNRAS*, 335, 965